Complex analysis in aeroacoustics

C. J. Chapman

Keele University

Presentation given at the Isaac Newton Institute,
Cambridge University

'Industrial Applications of Complex Analysis'

30 October 2019

What is aeroacoustics?

- Aeroacoustics is the study of sound generated aerodynamically.
- Leading example is sound generated by aircraft, especially the 'jet engine', i.e. high bypass-ratio turbofan.
- Other examples are noise from traffic (e.g. motorway noise), trains, wind turbines, ...
- Hugely important in civil life: controversies over where (and whether) to site new airports always involve noise.

Research in aeroacoustics

- Major research effort from
  - companies: Rolls-Royce, Boeing, ...
  - universities: Cambridge, Southampton, Boston, Florida, ...
  - government: NASA, EU, EPSRC, DLR, ONERA, ...
- Contribution from mathematicians:
  - Rayleigh
  - Lighthill, Curle, Hawkings
  - Howe, Crighton, Leppington, Dowling
  - Peake, Parry, CJC
  - Ayton, Brambley, Assier, Kisil, Baddoo, Priddin, Colbrook
- Thirteen from the Mathematics tripos at Cambridge.

A sister subject: hydroacoustics

- Hydroacoustics is the study of underwater sound.
- Includes ship and submarine noise, and sonar.
- Scientific principles are similar to aeroacoustics, but the Mach number is lower, and cavitation is important.
- Represented here today by Thales UK (D. Nigro).
- Fundamental for defence.
- Some researchers do both aero- and hydroacoustics.

A prototype aeroacoustic problem

One problem (out of many!) is that of a gust or turbulence striking the leading edge of an aeroengine fan blade or a wing.

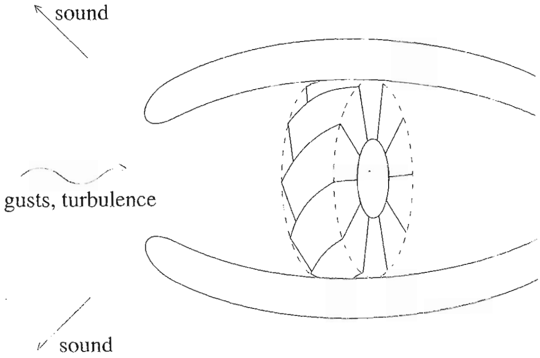

High-frequency sound is produced at the leading edges.

Lighthill's acoustic analogy (1952) (CJC 2015)

- Density perturbation in a sound wave satisfies

$$\left(\frac{\partial^2}{\partial t^2} - c_0^2\nabla^2\right)\rho' = \frac{\partial^2 T_{ij}}{\partial x_i \partial x_j}.$$

- The source (ignoring friction) is the acoustic stress tensor

$$T_{ij} = \rho u_i u_j + (p' - c_0^2\rho')\delta_{ij}.$$

- Radiated sound field is

$$p' = \frac{1}{4\pi}\frac{\partial^2}{\partial x_i \partial x_j}\int_{-\infty}^{\infty}\frac{T_{ij}(\mathbf{y}, t - |\mathbf{x}-\mathbf{y}|/c_0)}{|\mathbf{x}-\mathbf{y}|}\,\mathrm{d}^3\mathbf{y}.$$

Howe's vortex sound equation (1975) (CJC 2015)

- The Bernoulli variable B satisfies the vortex sound equation (for low Mach number)

$$\left(\frac{1}{c_0^2}\frac{\partial^2}{\partial t^2} - \nabla^2\right) B = \nabla \cdot (\boldsymbol{\omega} \wedge \mathbf{u}).$$

- The source is written in terms of the vorticity $\boldsymbol{\omega}$.

- The Bernoulli variable ('total enthalpy') is

$$B = \int \frac{\mathrm{d}p}{\rho} + \frac{1}{2}|\mathbf{u}|^2.$$

- The pressure in the radiated sound field is $p = \rho_0 B$.

Universality of complex analysis

- Most powerful representation is the (frequency, wavenumber) domain.
- Used by engineers, mathematicians, regulators (everyone!), because what matters is the spectrum.
- Given a function $f(x, y, z, t)$, write

$$f(x, y, z, t) = \iiiint F(\omega, k, l, m)\mathrm{e}^{-\mathrm{i}(\omega t - kx - ly - mz)}\,\mathrm{d}\omega\,\mathrm{d}k\,\mathrm{d}l\,\mathrm{d}m.$$

- Convention: capital letters for Fourier transform, i.e. the spectrum.

Universality of complex analysis

- A generic aeroacoustic equation is

$$\frac{1}{c_0^2}\left(\frac{\partial}{\partial t}+U\frac{\partial}{\partial x}\right)^2\varphi-\left(\frac{\partial^2}{\partial x^2}+\frac{\partial^2}{\partial y^2}+\frac{\partial^2}{\partial z^2}\right)\varphi=f(x,y,z,t).$$

- The source $f(x,y,z,t)$ has spectrum $F(\omega,k,l,m)$.
- Similarly, the field $\varphi(x,y,z,t)$ has spectrum $\Phi(\omega,k,l,m)$.
- Hence

$$D(\omega,k,l,m)\,\Phi(\omega,k,l,m)=F(\omega,k,l,m),$$

where $D(\omega,k,l,m)$ is the dispersion function.

- Therefore the solution of the aeroacoustic equation is

$$\Phi(\omega,k,l,m)=\frac{F(\omega,k,l,m)}{D(\omega,k,l,m)}.$$

Universality of complex analysis

- In the (space, time) domain, the solution of the aeroacoustic equation is

$$\varphi(x,y,z,t) = \iiiint \frac{F(\omega,k,l,m)}{D(\omega,k,l,m)} \mathrm{e}^{-\mathrm{i}(\omega t - kx - ly - mz)} \,\mathrm{d}\omega\,\mathrm{d}k\,\mathrm{d}l\,\mathrm{d}m.$$

- But what can be done with this 'inversion integral'? The initial range of integration is over real (ω,k,l,m).

- The field is 'coded' in the complex plane by local behaviour near special points, especially saddle points, branch points, poles, and their coalescences.

- Such points are accessible only by contour deformations taking full account of the global behaviour of F and D, especially their Riemann surfaces.

An example: scattering of vorticity into sound

Prototype problem is a gust or turbulence striking the leading edge of an aeroengine fan blade or a wing.

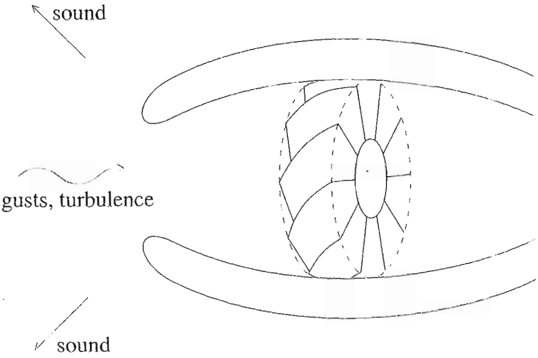

High-frequency sound is produced at the leading edges.

Leading edge geometry

Three coordinate systems based on leading edge:

- Cartesian: (x, y, z); wavenumbers (k, l, m)
- Cylindrical: (r, ϕ, x)
- Spherical: (R, θ, ϕ)

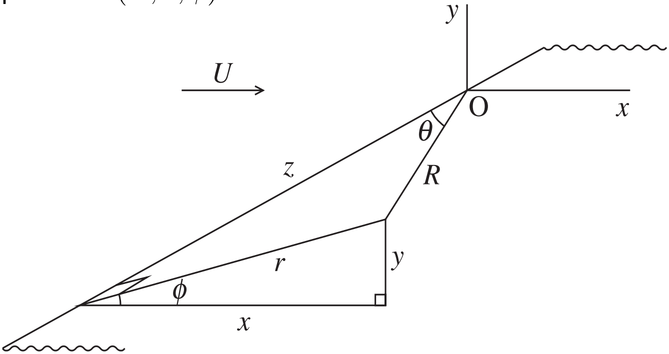

Localised gust: some basic questions

- What is the full three-dimensional directivity pattern of the radiated sound field?
- What happens on the leading edge, remote from the localised source, in quantitative detail?
- Is there a trapped wave propagating along the edge?
- What happens to the energy propagating along an edge when it comes to a corner (conical scattering)?
- Many detailed results can be obtained by complex analysis. These are not complete for corner scattering.

Single-frequency sesquipole

Let the upwash be

$$v_0 \mathrm{e}^{-\mathrm{i}\omega_0(t-x/U)}\delta(z/a).$$

Then the acoustic pressure is

$$p = \frac{\mathrm{e}^{-\pi\mathrm{i}/4}}{2\pi^{3/2}}\rho_0 c_0 \bar{v}_0 M^{3/2}\frac{\cos\frac{1}{2}\bar{\phi}}{\sin^{1/2}\bar{\theta}}\,\bar{a}\left(\frac{\omega_0}{c_0\bar{R}}\right)^{1/2}\mathrm{e}^{-\mathrm{i}\omega_0(t+M\bar{x}/c_0)}E_1,$$

where

$$E_1 = E_1(\omega_0\bar{R}/c_0,\bar{\theta},M) = \frac{\mathrm{i}}{\pi}\int_C \frac{\mathrm{e}^{\mathrm{i}(\omega_0\bar{R}/c_0)\cos(\bar{\theta}-\chi)}\sin\chi}{(1+M\sin\chi)^{1/2}}\,r'\chi.$$

Here E_1 is an 'edgelet' function.

Far field

The far-field approximation to E_1, uniform in the polar angle $\bar{\theta}$, is

$$E_1 \simeq \left(\tfrac{2}{\pi}\right)^{1/2} \frac{\sin\bar{\theta}}{(1+M\sin\bar{\theta})^{1/2}} \left\{1 + \frac{\mathrm{i}M}{2\sin\bar{\theta}}\frac{c_0}{\omega_0\bar{R}}\right\} \left(\frac{c_0}{\omega_0\bar{R}}\right)^{1/2} \mathrm{e}^{\mathrm{i}(\omega_0\bar{R}/c_0 - 3\pi/4)}.$$

Thus the dominant term is of order $\bar{R}^{-1/2}$, except along the leading edge, $\bar{\theta} = 0$ or π, where it is smaller, of order $\bar{R}^{-3/2}$.

Topology of $(1 + M \sin\chi)^{1/2}$ (CJC 2003)

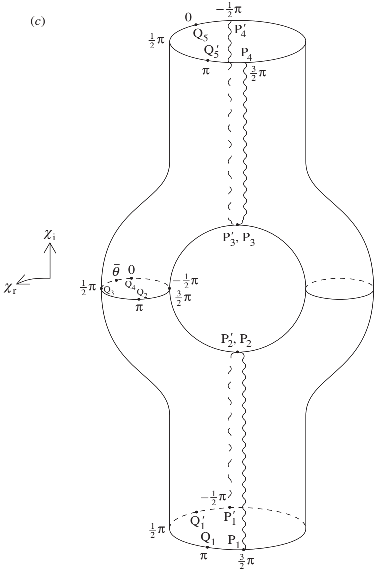

Contours on Riemann surface (CJC 2003)

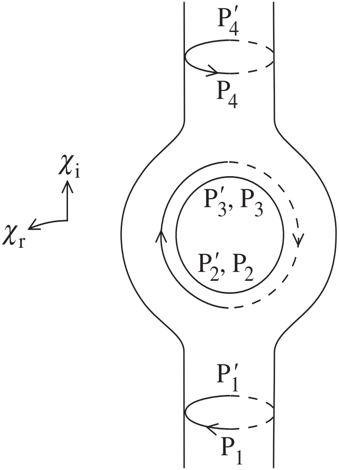

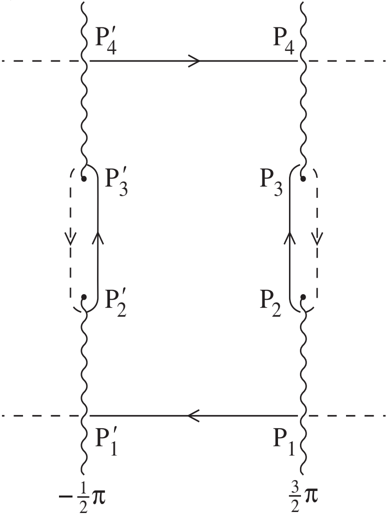

Detailed asymptotics (2013) (Ayton & Peake)

Wiener-Hopf method and advanced complex analysis

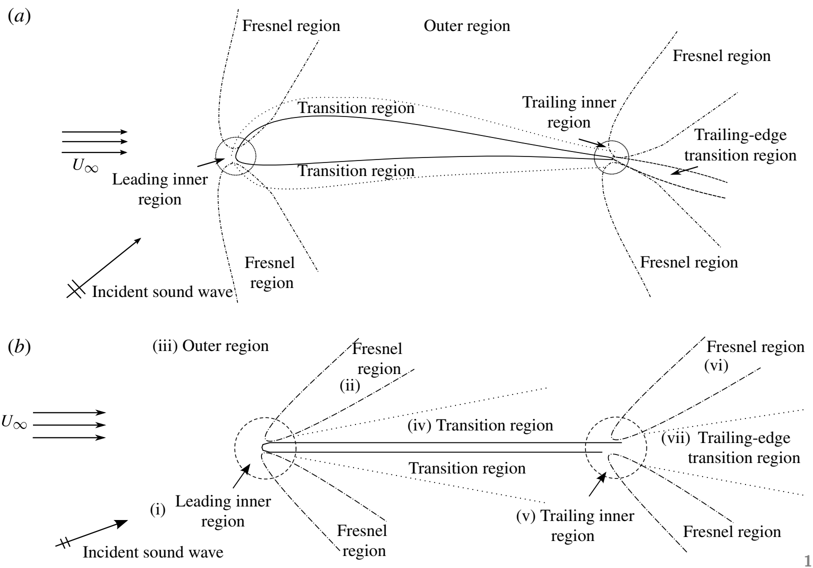

Parabolic wave equation (2019) (Hewitt et al.)

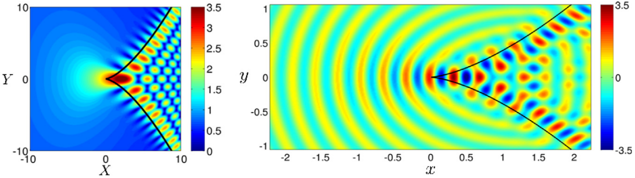

(a) $|A_{31}|$ (b) $\mathrm{Re}\left[A_{31}\mathrm{e}^{\mathrm{i}kx}\right]$

Fig. 9. Plots of $|A_{31}(X, Y)|$ and $\mathrm{Re}\left[A_{31}\mathrm{e}^{ikx}\right]$ for $(l, m) = (2, 1)$, with $\lambda = l/(l + 2m) = 1/2$ and $k = 20$. The curve near which the solution is localised is superimposed in black.

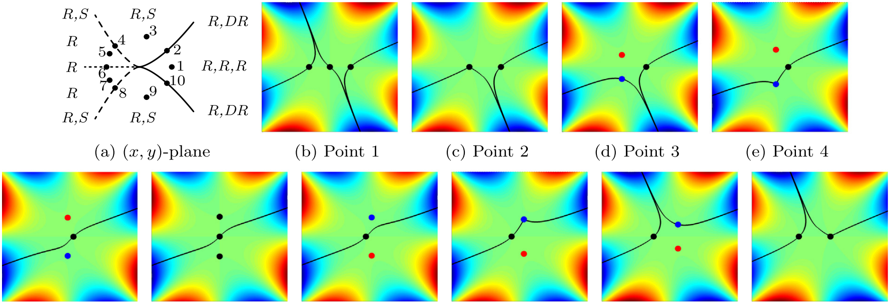

(a) (x, y)-plane (b) Point 1 (c) Point 2 (d) Point 3 (e) Point 4

(f) Point 5 (g) Point 6 (h) Point 7 (i) Point 8 (j) Point 9 (k) Point 10

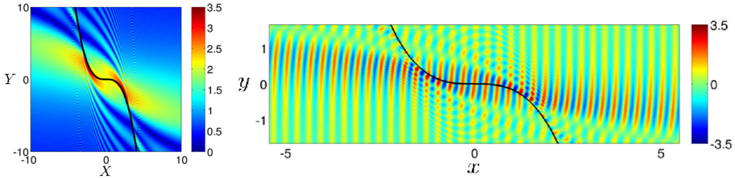

(a) $|A_{31}|$ (b) $\mathrm{Re}\left[A_{31}\mathrm{e}^{\mathrm{i}kx}\right]$

Fig. 13. Plots of $|A_{31}(X,Y)|$ and $\mathrm{Re}\left[A_{31}\mathrm{e}^{\mathrm{i}kx}\right]$ for $(l,m)=(1,2)$, with $\lambda = l/(l+2m) = 1/5$ and $k=20$. The curve near which the solution is localised is superimposed in black.

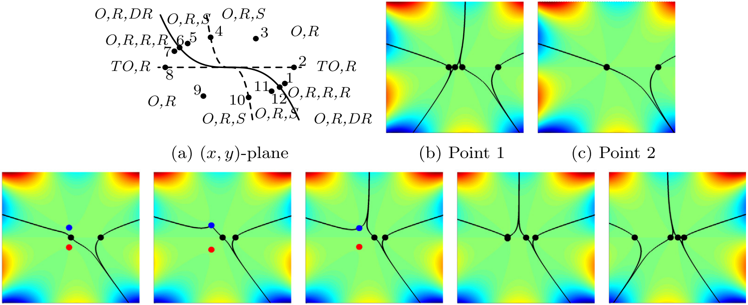

(a) (x,y)-plane (b) Point 1 (c) Point 2

(d) Point 3 (e) Point 4 (f) Point 5 (g) Point 6 (h) Point 7

Serrated trailing edge (2019) (Huang)

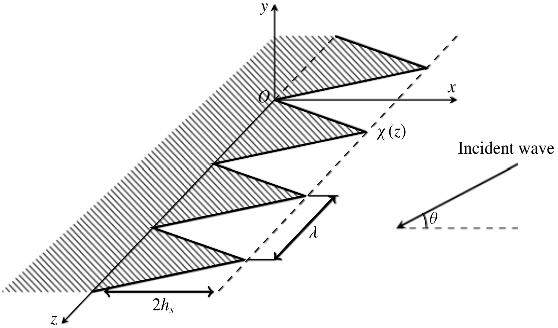

FIGURE 1. Sketch of the model problem. Here, x, y, z are the coordinates, O the origin, $\chi(z)$ the profile of serrations, $2h_s$ the root-to-tip distance and θ the incident angle.

Serrated trailing edge (2019) (Huang)

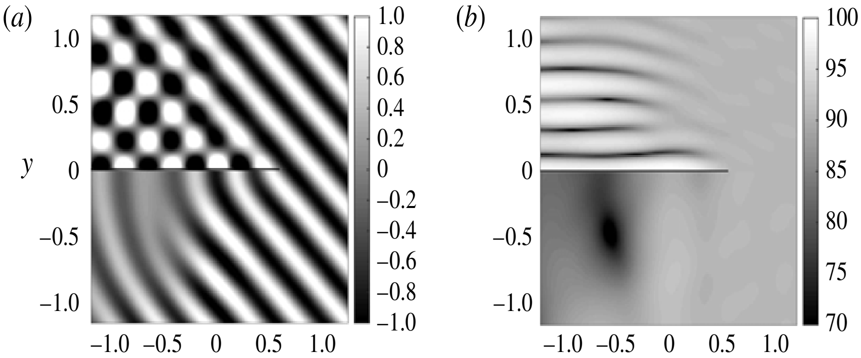

Silent flight of owls (2020) (Jaworski & Peake)

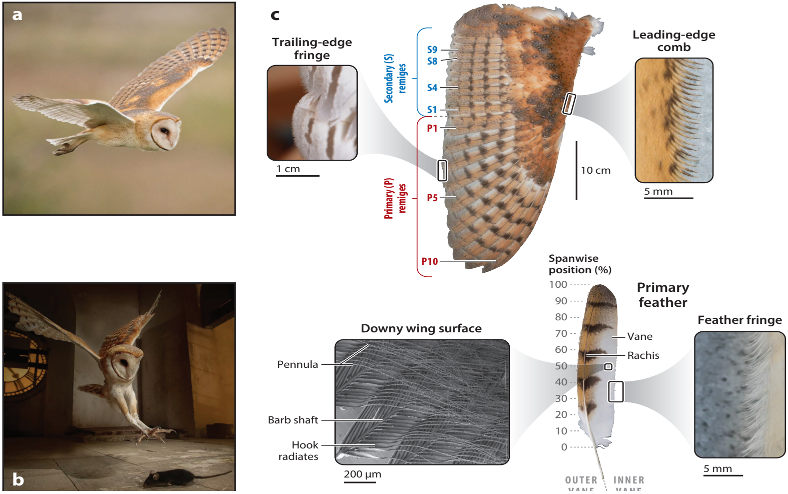

Silent flight of owls (2020) (Jaworski & Peake)

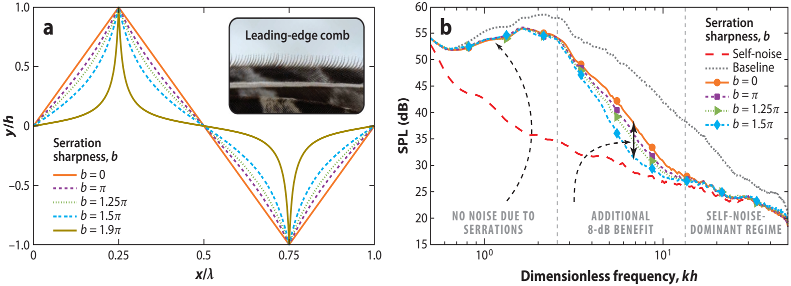

Figure 5

Aerodynamic noise suppression from leading-edge serrations and its dependence on geometry. (*a*) Serration geometries without stationary points are necessary to maximize leading-edge noise reduction. The sharpness of the serration with height h and wavelength λ is parameterized by b. (*Inset*) The pointed leading-edge comb of a long-eared owl. (*b*) Experimental measurements of sound pressure level (SPL) in the acoustic far field for a flat plate at zero angle of attack as a function of nondimensional frequency, with acoustic wave number k and height h. "Self-noise" refers to a serrated case ($b = 1.5\pi$) without upstream grid turbulence, and "baseline" refers to a straight leading edge case ($b = 0$) with grid turbulence. Grid turbulence intensity is 2.5%, with an integral length scale of approximately 6 mm. These serration geometries produce up to 8-dB noise reduction and the removal of leading-edge noise in the self-noise-dominant regime. Figure adapted with permission from Lyu et al. (2018).

Porous extension to trailing edge (2018) (Kisil & Ayton)

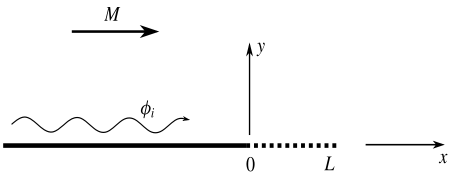

FIGURE 1. Diagram of the model problem: a semi-infinite rigid plate lies in $y = 0$, $x < 0$, and a finite porous plate lies in $y = 0$, $0 < x < L$. An unsteady perturbation, ϕ_i, convects with the mean flow in the positive x direction.

(i) a partial factorisation with exponential factors in the desired half-planes;
(ii) additive splitting of some terms;
(iii) application of Liouville's theorem;
(iv) iterative procedure to determine the remaining unknowns.

Porous extension to trailing edge (2018) (Kisil & Ayton)

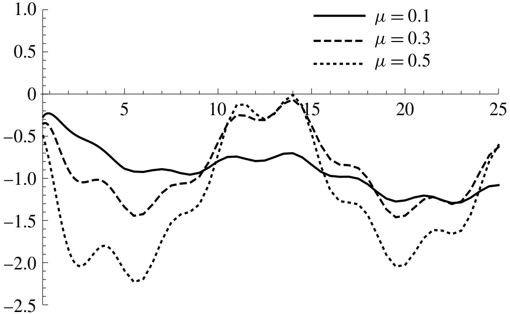

FIGURE 10. $\Delta P(k_0)$ for semi-infinite partially porous plates with varying porosity parameter, μ.

The quarter plane (2018) (Assier & Shanin)

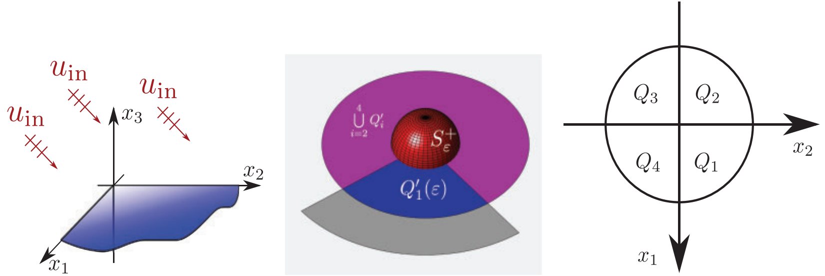

Fig. 1 (left) Geometry of the problem. (centre) 'Bottom lid' of $\Omega_{R,\varepsilon}$. The quarter-plane is in grey. (right) Illustration of the Q_i quadrants

The quarter plane (2018) (Assier & Shanin)

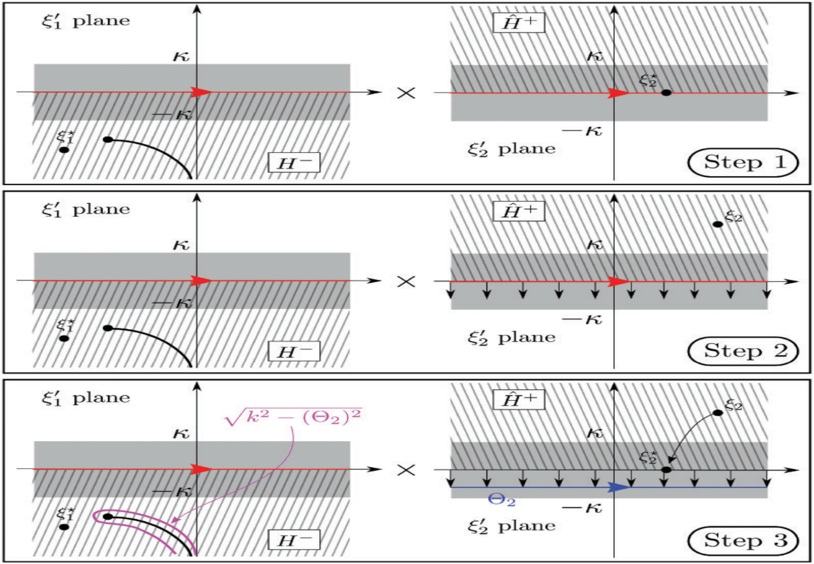

Fig. 6 Illustration of the contour deformation needed to prove analyticity on $\mathbb{H}^- \times \mathbb{R}$

Supersonic leading edge (2019) (Powles & CJC)

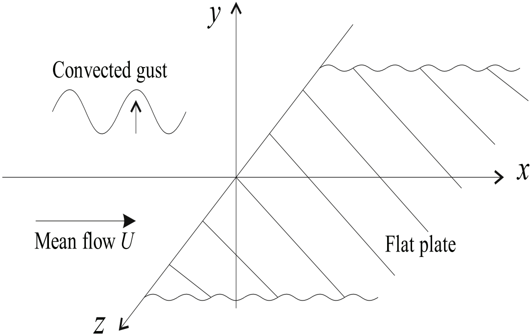

Fig. 1. Gust convected at speed U in the x-direction past a stationary flat-plate aerofoil. The aerofoil occupies the half-plane $y = 0$, $x \geq 0$, and the leading edge lies along the z-axis.

Supersonic leading edge (2019) (Powles & CJC)

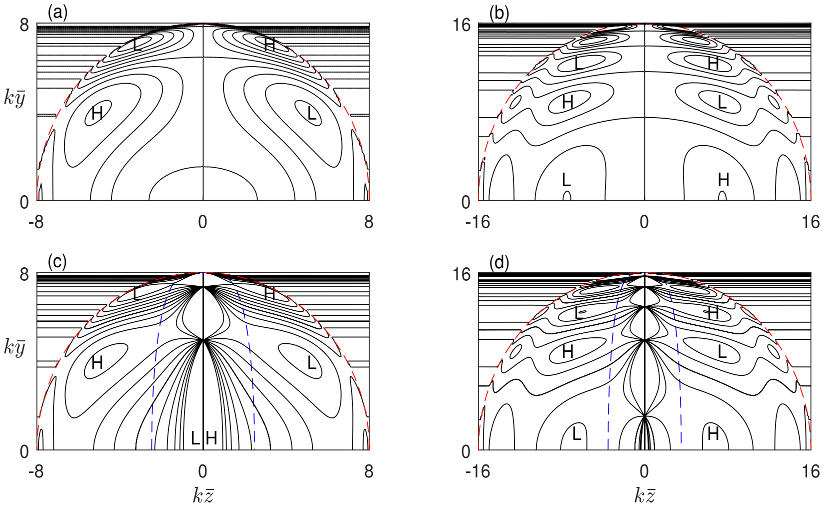

Fig. 4. Scaled pressure contours on transverse vertical sections for an anti-symmetric gust convected at Mach number $M = \sqrt{2}$. (a) accurate plot on $k\bar{x} = 8$ from Eq. (11); (b) accurate plot on $k\bar{x} = 16$; (c) Keller approximation to (a), using Eq. (21) with coefficients (26); (d) Keller approximation to (b). Contour values in (a), (c) are -0.5 to 0.5, and in (b), (d) are -0.25 to 0.25, marked low (L) to high (H). The dashed semi-circles are sections of the Mach cone $\bar{R}_h = 0$, and the dashed half-ovals are sections of the surface (28) for $\sigma = 0.5$, outside of which the Keller approximation applies. In (c), (d) the Keller approximation has a singular limit $\pm\infty$ along the vertical axis $z = 0$.

References

Assier, R. C. & Shanin, A. V. (2018) Diffraction by a quarter-plane. Analytical continuation of spectral functions. *Q. Jl Mech. Appl. Math.* **72**, 51–86.

Ayton, L. J. & Peake, N. (2013) On high-frequency noise scattering by aerofoils in flow. *J. Fluid Mech.* **734**, 144–182.

Chapman, C. J. (2003) High-speed leading-edge noise. *Proc. R. Soc. Lond. A* **459**, 2131–2151.

Chapman, C.J. (2015) Aircraft noise. *Princeton Companion to Applied Mathematics* (Princeton University Press), pp. 197–201.

Chapman, C. J. & Powles, C. J. (2019) Basic singular fields in the theory of impulsive supersonic leading-edge noise. *Wave Motion* **89**, 79–92.

References (continued)

Hewett, D. P., Ockendon, J. R. & Smyshlyaev. V. P. (2019) Contour integral solutions of the parabolic wave equation. *Wave Motion* **84**, 90–109.

Huang, X. (2017) Theoretical model of acoustic scattering from a flat plate with serrations. *J. Fluid Mech.* **819**, 228–257.

Jaworski, J. W. & Peake, N. (2020) Aeroacoustics of silent owl flight. *Annual Review of Fluid Mechanics* **52**, 395–420.

Kisil, A. & Ayton, L. J. (2018) Aerodynamic noise from rigid trailing edges with finite porous extensions. *J. Fluid Mech.* **836**, 117–144.

Powles, C. J. & Chapman, C. J. (2019) Canonical sound fields in the frequency-domain theory of supersonic leading-edge noise. *Wave Motion* **86**, 125–136.